



저작자표시-비영리-변경금지 2.0 대한민국

이용자는 아래의 조건을 따르는 경우에 한하여 자유롭게

- 이 저작물을 복제, 배포, 전송, 전시, 공연 및 방송할 수 있습니다.

다음과 같은 조건을 따라야 합니다:



저작자표시. 귀하는 원저작자를 표시하여야 합니다.



비영리. 귀하는 이 저작물을 영리 목적으로 이용할 수 없습니다.



변경금지. 귀하는 이 저작물을 개작, 변형 또는 가공할 수 없습니다.

- 귀하는, 이 저작물의 재이용이나 배포의 경우, 이 저작물에 적용된 이용허락조건을 명확하게 나타내어야 합니다.
- 저작권자로부터 별도의 허가를 받으면 이러한 조건들은 적용되지 않습니다.

저작권법에 따른 이용자의 권리는 위의 내용에 의하여 영향을 받지 않습니다.

이것은 [이용허락규약\(Legal Code\)](#)을 이해하기 쉽게 요약한 것입니다.

[Disclaimer](#)

의학박사 학위논문

**Suppression of experimental choroidal
neovascularization in a rat model by
a telomerase-derived peptide vaccine**

실험적 맥락막신생혈관 쥐 모델에서 텔로머레이즈
유래 펩타이드 백신의 억제효과

2021 년 2 월

서울대학교 대학원

의학과 안과학 전공

이 은 경










Suppression of experimental choroidal neovascularization in a rat model by a telomerase-derived peptide vaccine

지도교수 유 형 곤

이 논문을 의학박사 학위논문으로 제출함
2020 년 10 월

서울대학교 대학원
의학과 안과학 전공
이 은 경

이은경의 의학박사 학위논문을 인준함
2021 년 1 월

위원장		 (인)
부위원장		 (인)
위원		 (인)
위원		 (인)
위원	변석호	 (인)

ABSTRACT

Suppression of experimental choroidal neovascularization in a rat model by a telomerase-derived peptide vaccine

Eun Kyoung Lee

Ophthalmology, College of Medicine

The Graduate School

Seoul National University

Purpose: The choroidal neovascularization (CNV) is the main pathogenic process in neovascular age-related macular degeneration (AMD). CNV formation occurs by a complex mechanism involving oxidative stress and inflammation as well as vascular endothelial growth factor (VEGF)-related angiogenic stimuli. In current study, we investigated the effect of GV1001, a novel peptide derived from human telomerase reverse transcriptase, on experimental CNV.

Methods: Experimental CNV was induced by laser photocoagulation in Brown Norway rats. GV1001 was subcutaneously administered (0.1 nM, 1 nM, and 10 nM) daily, beginning 3 days prior, and ending 14 days after laser injury. Optical coherence tomography, fluorescein angiography, and choroidal flat mount were performed to analyze CNV. To determine the mechanism by which GV1001 acted, the protein level of inhibitor of nuclear factor kappa B- α (I κ B- α) and nuclear translocation of nuclear factor kappa B (NF- κ B) was analyzed via immunohistochemistry of p65.

Multiplex immunoassay was also performed to evaluate the interleukin (IL)-1 β , IL-6, VEGF, monocyte chemotactic protein (MCP)-1, and tumor necrosis factor (TNF)- α levels.

Results: The GV1001-treated group had significantly lower CNV thickness ($P < 0.001$), smaller CNV area ($P < 0.001$), and lower proportion of CNV lesions with clinically significant fluorescein leakage ($P < 0.001$) than vehicle-treated group, with the highest inhibitory effect at 1 nM concentration. GV1001 treatment inhibited I κ B- α degradation ($P < 0.05$) and NF- κ B p65 nuclear translocation ($P < 0.01$). 1 nM GV1001 treatment significantly suppressed the levels of IL-1 β ($P < 0.001$), IL-6 ($P < 0.001$), and VEGF ($P = 0.005$).

Conclusions: Systemic administration of GV1001 led to significant suppression of laser-induced CNV, alongside inhibition of inflammatory processes including NF- κ B activation and subsequent upregulation of pro-inflammatory cytokines. This study demonstrates the molecular evidence of potential validity of these novel drug candidates as a reasonable therapeutic adjuvant strategy for treating neovascular AMD.

Keyword: Age-related macular degeneration, Choroidal neovascularization, GV1001, NF- κ B pathway, Peptide, Telomerase, Vaccine.

Student Number: 2013-31144

TABLE OF CONTENTS

Abstract	i
Table of Contents	iii
List of Figures	v
List of Abbreviations	vii
Introduction	1
Materials and Methods	5
1. Group classification according to the administration of GV1001 peptide and control vehicle	5
2. Laser-induced choroidal neovascularization.....	6
3. Optical coherence tomography	6
4. Flat mount staining and choroidal neovascularization size measurement	7
5. Fluorescein angiography	7
6. Western blot analysis for I κ B- α , phospho-I κ B- α , and phospho-NF- κ B p65	8
7. Immunohistochemistry for NF- κ B p65.....	9
8. Quantification of cytokines	9
9. Telomerase activity in CNV	10

10. Statistical analysis.....	10
Results.....	14
1. Inhibitory effect of GV1001 on laser-induced CNV; Quantification of CNV	14
2. Anti-angiogenic effect of GV1001 on CNV; Angiographic leakage from CNV	14
3. Inhibition of NF-κB activation in vivo by treatment with GV1001 	15
4. Effect of GV1001 on pro-inflammatory cytokines production...	16
5. Telomerase activity in CNV	17
Discussion	27
References.....	36
Abstract in Korean	42

LIST OF FIGURES

Figure 1. Experimental schedules to evaluate the effect of GV1001	
in laser-induced CNV rat model.....	12
Figure 2. The CNV lesions with hemorrhagic complication.....	13
Figure 3. Spectral-domain optical coherence tomography images of	
CNV.....	18
Figure 4. Fluorescent images of CNV in retinal pigment epithelium-	
choroid-scleral flat mounts	19
Figure 5. Fluorescein angiographic images.....	20
Figure 6. In vivo inhibition of nuclear translocation of NF-κB p65	
by treatment with GV1001.....	22
Figure 7. The suppression of NF-κB activation by treatment with	
GV1001 using western blot	24
Figure 8. Quantification of IL-1β, IL-6, VEGF, MCP-1, and TNF-α	
levels in RPE-choroid complex	25
Figure 9. Immunohistochemical staining of hTERT expression in	
paraffin-embedded rat eye sections through areas of CNV	
.....	26
Figure 10. Schematic diagram of the NF-κB signaling pathway	
suppressed by GV1001	34
Figure 11. Comparison of the mean CNV area and the mean largest	

CNV lesion diameter between GV1001-treated group and aflibercept-treated group	35
---	-----------

LIST OF ABBREVIATIONS

CNV, choroidal neovascularization

AMD, age-related macular degeneration

RPE, retinal pigment epithelium

IL, interleukin

MCP, monocyte chemotactic protein

TNF, tumor necrosis factor

VEGF, vascular endothelial growth factor

RNA, ribonucleic acid

DNA, deoxyribonucleic acid

hTERT, human telomerase reverse transcriptase

APCs, antigen presenting cells

HLA, human leukocyte antigen

IFN, interferon

HSPs, heat shock proteins

GnRHR, gonadotropin-releasing hormone receptor

NF- κ B, nuclear factor kappa B

ARVO, Association for Research in Vision and Ophthalmology

IACUC, Institutional Animal Care and Use Committee

PBS, phosphate buffered saline

OCT, optical coherence tomography

SD-OCT, spectral domain-optical coherence tomography

FITC, fluorescein isothiocyanate

FA, fluorescein angiography

SDS-PAGE, sodium dodecyl sulphate–polyacrylamide gel electrophoresis

PVDF, polyvinylidene fluoride

RT, room temperature

I κ B- α , inhibitor of nuclear factor kappa B- α

HRP, horseradish peroxidase

ARPE-19, human adult retinal pigment epithelial cells

GM-CSF, granulocyte macrophage-colony stimulating factor

INTRODUCTION

Choroidal neovascularization (CNV) is the main pathogenic process and a leading cause of severe vision loss in neovascular age-related macular degeneration (AMD) patients. Molecular and cellular mechanisms underlying CNV are not fully elucidated. CNV seen in AMD develops with chronic inflammation adjacent to the retinal pigment epithelium (RPE), Bruch's membrane, and choriocapillaris. As inflammation and oxidative stress have been advocated to play an important role in CNV development, several inflammation and oxidative stress markers have been investigated. Inflammatory cytokines, such as interleukin (IL)-1 β ,¹ IL-6,² monocyte chemoattractant protein (MCP)-1,³ and tumor necrosis factor (TNF)- α ⁴ are reported to play a role in CNV development. Besides its involvement in inflammatory mechanisms, various clinical studies have shown that vascular endothelial growth factor (VEGF) plays a central role in CNV pathogenesis. Nevertheless, much of the CNV pathogenesis remains to be elucidated.

Telomerase is a ribonucleoprotein enzyme, which mediates the ribonucleic acid (RNA)-dependent synthesis of telomeric deoxyribonucleic acid (DNA), protecting chromosome ends.⁵ Under normal conditions telomerase is expressed in embryonic cells, bone marrow stem cells and in the colonic crypt.⁶⁻⁸ During repeated rounds of DNA replication, telomeres become progressively shorter and without a compensating mechanism, cells enter senescence and eventually die.⁷⁻⁹ In the vast majority of cancer cells, telomerase reactivation is a key event in transformation of a normal cell into a malignant cell, acting as a mechanism which confers cancer cell immortality.^{6,7,10,11} GV1001, a peptide composed of 16 amino acids (Glu-Ala-Arg-

Pro-Ala-Leu-Leu-Thr-Ser-Arg-Leu-Arg-Phe-Ile-Pro-Lys), is derived from the human telomerase reverse transcriptase (hTERT) catalytic subunit.¹² It was originally developed as a chemotherapeutic drug for the treatment of various types of cancer, including advanced pancreatic cancer,^{13,14} melanoma,¹⁵ non-small cell lung cancer,^{16,17} and advanced hepatocellular carcinoma.¹⁸ GV1001 is provided as a lyophilized peptide for intradermal injection. The mechanism of action of GV1001 depends on peptide uptake by antigen presenting cells (APCs) in the skin, migration of these cells to regional lymph nodes, and effective presentation of GV1001-associated epitopes to immune cells.¹⁹ Even though it is not fully elucidated, the mode of action as currently understood is that it binds multiple human leukocyte antigen (HLA) class II molecules and harbors putative HLA class I epitopes.¹⁹ Consequently, GV1001 may elicit combined CD4 and CD8 T-cell responses, which are crucial for initiating tumor eradication. The activity of CD4 T cells at the tumor site lead to a secretion of interferon (IFN)- γ and IL-2, further stimulating CD8 cytotoxic T cells and natural killer cells, which may help to increase the infiltration and the retention of CD8 T-cells into the tumor sites leading to upregulation and re-expression of MHC class I molecules.⁵

Additionally, GV1001 is reported to interact with various cellular proteins and receptors such as heat shock proteins (HSPs); as it can penetrate the plasma membranes of cells and can be localized in the cytoplasm.²⁰ HSPs have been recognized as intracellular molecular chaperones that can be induced by diverse stresses to cells.²¹ Previous studies have demonstrated that these molecules can be localized at the plasma membrane and released into extracellular space under physiological conditions.²²⁻²⁴ Among these proteins, HSP90 is a ubiquitously

expressed molecular chaperone, whereas HSP70 is highly induced by different stresses such as heat, oxidative stress, or anticancer drugs.²⁵ Both HSP70 and HSP90 have been found to be localized in the plasma membrane and extracellular space. They are capable of delivering peptides to APCs by receptor-mediated endocytosis.²⁶ Lee et al.²⁷ have shown that GV1001 may internalize into cells by HSP70 and HSP90 mediated endocytosis. They demonstrated that treatment of anti-HSP70 and HSP90 antibodies lowered the internalization of GV1001. Furthermore, GV1001 is reported to physically interact with gonadotropin-releasing hormone receptor (GnRHR) and affects the downstream signaling pathways,²⁸ as well as efficiently enters neural stem cells under normal conditions and is predominantly localized in the cytoplasm and mitochondria.²⁹ Various biological functions of GV1001, such as, antioxidant effect against ischemia-reperfusion injury,³⁰⁻³² anti-inflammatory effects via the regulation of nuclear factor kappa B (NF- κ B) signaling pathway,^{33,34} and neuroprotective effects against beta amyloid,²⁹ as well as anti-cancer effects have been reported and these functions may be attributed to the various interactions of GV1001 with cellular proteins.

The degeneration of RPE is considered as the hallmark of AMD. With increase in age, there is accumulation of lipofuscin in the RPE, the phagocytosis capacity of RPE deteriorates, and the oxidative stress induces even more senescence. Cultured human RPE cells transfected with hTERT were found to be resistant to senescence and do not express senescence-associated beta-galactosidase activity.³⁵ Based on this, hTERT-based therapy may have therapeutic benefits in AMD patients. In this study, the effect of GV1001 on laser-induced CNV in a rat model was investigated to explore its application as a new therapeutic strategy for AMD-

associated CNV. In addition, the protective mechanism by which GV1001 suppresses laser-induced CNV was also investigated.

MATERIALS AND METHODS

This study adhered to the Association for Research in Vision and Ophthalmology (ARVO) Statement regarding the Use of Animals in Ophthalmic and Vision Research. All procedures and study protocol was approved by the Institutional Animal Care and Use Committee (IACUC) of the Clinical Research Institute at Seoul National University Hospital (Permit number: 13-0279)

Male Brown Norway rats (Japan SLC, Hamamatsu, Japan) aged 7 weeks, weighing 160–180 g, were used in this study. During all procedures, including examination and photography, rats were anesthetized with a 1:1 ketamine hydrochloride (Phoenix Pharmaceutical, St. Joseph, MO): xylazine hydrochloride (Phoenix Pharmaceutical) mixture (1 mL/kg) that was administered intramuscularly and all efforts were made to minimize suffering. Pupils were dilated with tropicamide (0.5% Mydrin M, Santen Pharmaceutical, Osaka, Japan).

Group classification according to the administration of GV1001 peptide and control vehicle

GemVax & KAEL (Seongnam, Gyeonggi-do, South Korea) supplied GV1001 peptide (1.868 kDa). Animals were randomly divided into four groups, according to GV1001 concentrations, as vehicle only (control), 0.1 nM (0.1868 µg/kg), 1 nM (1.868 µg/kg), and 10 nM (18.68 µg/kg). GV1001 was dissolved in phosphate buffered saline (PBS), and GV1001 or PBS was subcutaneously administered. Three days before laser photocoagulation, all rats began receiving either GV1001 or vehicle once a day, which continued for 14 days after laser photocoagulation (Figure

1). The overall health of each rat was evaluated by assessing its weight, general appearance, alertness, and skin abnormalities at the injection site. All rats remained alert and responsive during the study periods, and there was no evidence of adverse effects such as weight change or skin abnormalities.

Laser-induced choroidal neovascularization

After rats were anesthetized and pupils were dilated, rats were positioned on a Mayo stand in front of a laser-delivery system. The fundus was visualized using a cover slip with 0.3% hydroxypropyl-methylcellulose (Genteal, Novartis Ophthalmics, Duluth, GA) as an optical coupling agent. A diode laser (Supra 577.Y, Quantel Medical SAS, Clermont-Ferrand, France) was used for photocoagulation (577 nm wavelength, 0.05 seconds duration, 100 μ m spot size, 150 mW power). Seven to eight lesions were generated approximately 2-3 disc diameters from the optic disc, between the major retinal vessels. Bubble formation at the center of photocoagulation in the laser spotted zone indicated rupture of Bruch's membrane and creation of an injury sufficient to induce CNV. Spots with hemorrhagic complications were excluded from further evaluation (Figure 2).

Optical coherence tomography

Optical coherence tomography (OCT) was performed on anesthetized rats, using a spectral domain-optical coherence tomography (SD-OCT) system (Cirrus OCT, Carl Zeiss Meditec, Dublin, CA), 14 days following laser injury. The CNV was represented on OCT as a spindle-shaped, subretinal, hyper-reflective material above the RPE layer. The horizontal and vertical cross-sectional images of the CNV lesion

were obtained using a 5-line raster scan mode with length of 6 mm. The greatest linear dimension of the CNV lesion was measured using Cirrus OCT software.

Flat mount staining and choroidal neovascularization size measurement

The CNV lesion area was measured in RPE-choroid-sclera flat mounts. Fourteen days following laser photocoagulation, rats were anesthetized and perfused with 5 mL PBS containing 50 mg/mL of fluorescein isothiocyanate (FITC)-labeled dextran (Sigma-Aldrich, St. Louis, MO). The eyes of rats were then enucleated and fixed for 1 hour in 4% phosphate-buffered paraformaldehyde. The anterior segment was removed, and the entire retina was carefully dissected from the eye cup. The RPE-choroid complex was flattened by making four radial incisions with the sclera facing down. Flat mounts were examined under a laser confocal microscope (LSM 510 META, Carl Zeiss, Jena, Germany) and images of laser-induced lesions were captured. The CNV lesions were identified as fluorescent blood vessels on the choroidal-retinal interface surrounded by a region with no fluorescence. An operator masked to assignment of treatment group, used images to measure CNV area in each laser burn using Carl Zeiss LSM Image Browser software (version 4.0.0.241).

Fluorescein angiography

Fluorescein angiography (FA) was performed on anesthetized animals, using an Optos 200Tx ultra-wide field retinal imaging system (Optos PLC, Dunfermline, Scotland, UK), 14 days following laser injury. Photographic images were captured after 0.4 mL of 10% fluorescein sodium solution (Alcon Laboratories, Inc., Fort Worth, TX) was injected into the peritoneum. Two masked retinal specialists, not

involved in laser photocoagulation or angiography, evaluated FA images. Lesions were graded using a previously established grading system.³⁶ Grade 2B lesions were regarded as clinically significant. Grade 0 lesions were excluded from analyses because the laser injury may not have been sufficient to induce CNV.

Western blot analysis for I κ B- α , phospho-I κ B- α , and phospho-NF- κ B p65

To determine whether GV1001 treatment affected the NF- κ B signaling pathway in the laser-induced CNV model, protein extracts were obtained from the homogenized RPE-choroid complex, 4 hours after laser photocoagulation. Proteins were extracted from cells using PRO-PREP protein extraction solution (Intron, Seoul, Korea). The protein concentration of each sample was measured by the BCA Protein Assay Kit (Pierce, Rockford, IL) using bovine serum albumin as the standard. Each sample containing 20 μ g of total protein was separated by sodium dodecyl sulphate–polyacrylamide gel electrophoresis (SDS-PAGE) and transferred to a polyvinylidene fluoride (PVDF) membrane. After blocking nonspecific binding with 5% skim milk in PBS for 1 hour at room temperature (RT), the membranes were incubated with monoclonal antibodies against inhibitor of nuclear factor kappa B- α (I κ B- α ; Cell signaling Technology, Beverly, MA), phospho-I κ B- α (Cell signaling), phospho-NF- κ B p65 (Cell signaling), or with monoclonal anti- β -actin antibody (Sigma-Aldrich) at 4°C overnight. The membranes were then incubated with anti-rabbit horseradish peroxidase (HRP) (Cell signaling) or anti-mouse HRP (Cell signaling) for 1 hour at RT. Signals were visualized using the SuperSignal West Pico chemiluminescent substrate (Perbio, Bonn, Germany) according to the manufacturer’s protocol.

Immunohistochemistry for NF- κ B p65

Paraffin sections of rat eyes were deparaffinized 4 hours after laser photocoagulation. The sections were then processed in 10 mM citrate buffer (pH 6.0) and heated in an autoclave for 10 min for antigen retrieval. Non-specific binding sites were blocked by incubating the sections with 10% normal goat serum (Abcam, Cambridge, UK) for 2 hours at RT. The sections were subsequently incubated with a rabbit polyclonal antibody against human NF- κ B p65 (Abcam) at 4°C overnight. The secondary antibody used was Alexa Fluor® goat anti-rabbit 488 (Invitrogen, Carlsbad, CA). The samples were then treated with TOTO-3 (Invitrogen) for nuclear staining and observed using a confocal microscope. For each sample, the average ratio of the number of cells with nuclear p65 staining to that of total cells per microscopic field was analyzed.

Quantification of cytokines

A multiplex immunoassay was performed to measure the concentrations of multiple cytokines, IL-1 β set (cat #171L1008M), IL-6 set (cat #171L1012M), VEGF set (cat #171L1-26M), MCP-1 set (cat # 171L1027M), and TNF- α set (cat #171L1025M). Proteins were extracted from the homogenized RPE-choroid complexes at the point when the expression of each cytokine was expected to be highest following laser photocoagulation; 10 hours for IL-1 β , 3 days for IL-6, VEGF, MCP-1, and 7 days for TNF- α . Multiplex immunoassay was performed using Bio-Plex® Pro assays (BIO-RAD Laboratories, Hercules, CA) using Luminex-bead-based xMAP technology according to the manufacturer's instruction. The antibody specific to each factor was covalently coupled to a different magnetic microsphere that was

uniquely labeled with a fluorescent dye. The microspheres were incubated with standards and samples in a 96-well microtiter plate at 850 rpm for 30 minutes at RT. After washing with wash buffer, diluted biotinylated secondary antibody was added to appropriate wells and incubated at 850 rpm for 30 minutes. After washing, streptavidin-phycoerythrin (Streptavidin-PE) conjugate was added to each well and incubated for 10 minutes. A final wash removed unbound Streptavidin-PE and the microspheres were resuspended in buffer and analyzed using Bio-Plex® multiplex system to determine the concentration of each biomarker. All the samples were diluted to minimum 4-fold.

Telomerase activity in CNV

Fourteen days after CNV induction, eyes were enucleated and immediately immersed in a mixture of 2.5% glutaraldehyde and 4% paraformaldehyde for 24 hours. Tissue samples were dehydrated and embedded in paraffin. Serial sections, 4- μ m thick, were then cut with a microtome and examined to determine the center of each lesion. The sections were evaluated for immunohistochemical analysis using a rabbit polyclonal antibody against hTERT (Abcam) to determine whether the mechanism of GV1001 is related to the telomerase activity in CNV.

Statistical analysis

The data are expressed as mean \pm standard deviation, where applicable. Statistical analyses were performed using the Kruskal-Wallis test for comparison between several groups and the Mann-Whitney *U* test for comparison between two subgroups to assess the effects of drug treatment. Statistical significance was defined as $P <$

0.05. All statistical analyses were performed using SPSS software for Windows (version 21.0, SPSS, Inc., Chicago, IL).

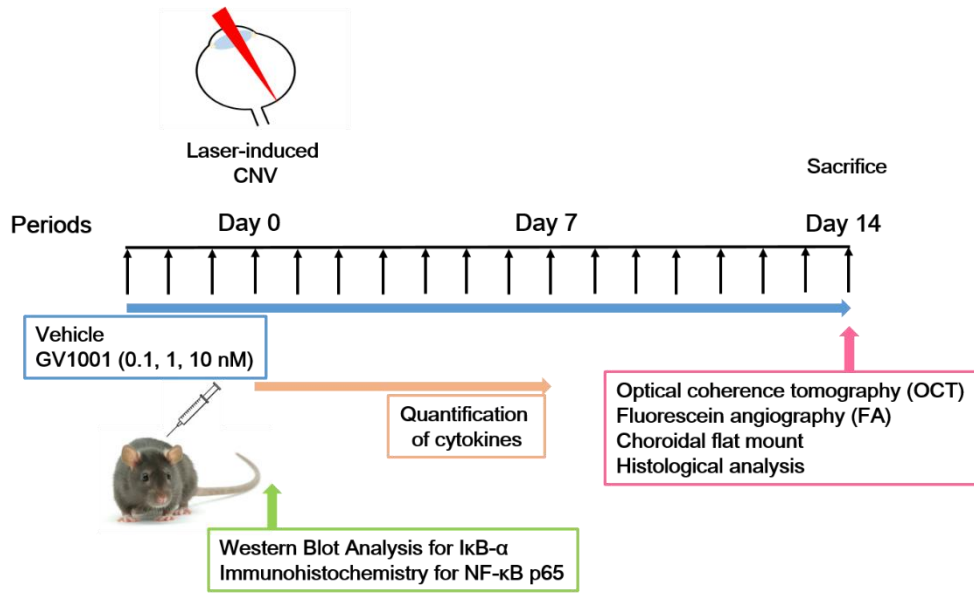


Figure 1. Experimental schedules to evaluate the effect of GV1001 in laser-induced CNV rat model. GV1001 or vehicle was subcutaneously administered once a day, beginning 3 days before laser photocoagulation and ending 14 days after laser photocoagulation.

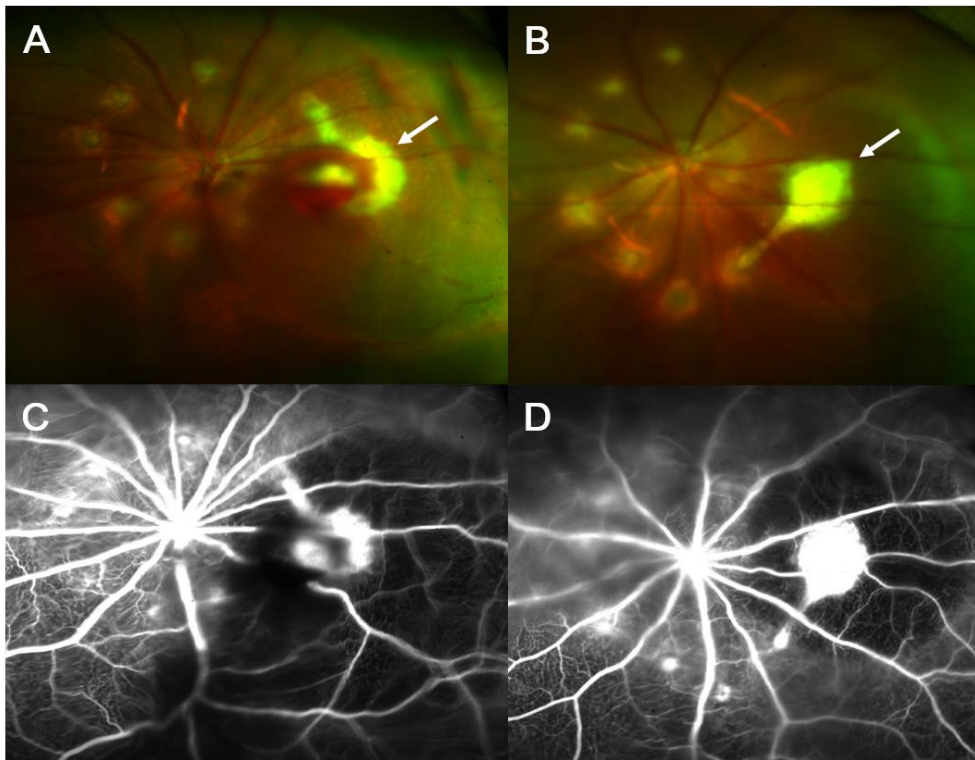


Figure 2. The CNV lesions that hemorrhagic complication occurred were excluded from the analysis (white arrows). Blocked fluorescence in fluorescein angiography demonstrates hemorrhage more clearly.

RESULTS

Inhibitory effect of GV1001 on laser-induced CNV; Quantification of CNV

SD-OCT images were obtained 14 days after laser photocoagulation to examine the effect of GV1001 on CNV lesion thickness. Mean CNV thickness was significantly reduced after GV1001 treatment (Figure 3). The mean CNV thickness was $103.85 \pm 16.53 \mu\text{m}$ in vehicle-treated group. It significantly decreased in GV1001-treated group at the concentrations, 0.1 nM ($80.90 \pm 13.19 \mu\text{m}$), 1 nM ($76.56 \pm 12.28 \mu\text{m}$), and 10 nM ($88.51 \pm 14.37 \mu\text{m}$) ($P < 0.001$, for all groups). The difference in CNV thickness between GV1001-treated groups (0.1 nM vs. 10 nM, $P = 0.013$; 1 nM vs. 10 nM, $P = 0.004$) was also statistically significant.

An analysis of choroidal flat mounts showed the distinct reduction in CNV area after GV1001 treatment (Figure 4). The mean CNV area was $39,203.82 \pm 8,920.27 \mu\text{m}^2$ in vehicle-treated group. It significantly decreased in GV1001-treated group at the concentrations, 0.1 nM ($25,356.89 \pm 6,961.43 \mu\text{m}^2$), 1 nM ($20,214.42 \pm 7,417.81 \mu\text{m}^2$), and 10 nM ($28,212.59 \pm 7,992.48 \mu\text{m}^2$) ($P < 0.001$, for all groups). The difference in CNV area between GV1001-treated groups (0.1 nM vs. 1 nM, $P = 0.001$; 1 nM vs. 10 nM, $P < 0.001$) was also statistically significant.

Anti-angiogenic effect of GV1001 on CNV; Angiographic leakage from CNV

To evaluate the *in vivo* effect of GV1001 on angiogenesis, FA was performed 14 days after laser photocoagulation. Comparison of angiograms between groups confirmed that angiographic leakage from CNV was less severe in GV1001-treated groups. Figure 5 illustrates the proportion of CNV lesions with fluorescein leakage in each

group. Pathologically significant leakage (grade 2B lesions) was observed in 66.1% of the vehicle-treated group. It significantly decreased in GV1001-treated group at the concentrations, 0.1 nM (37.9%), 1 nM (21.1%), and 10 nM (21.4%) ($P < 0.001$ for all groups). The difference in the proportion of grade 2B lesions between GV1001-treated groups (0.1 nM vs. 1 nM, $P = 0.031$; 0.1 nM vs. 10 nM, $P = 0.035$) was also statistically significant.

Inhibition of NF- κ B activation in vivo by treatment with GV1001

To define the signaling pathway involved in the treatment with GV1001, we focused on NF- κ B as an upstream transcriptional factor of inflammatory mediators and analyzed the protein level of I κ B- α and nuclear translocation of NF- κ B p65 *in vivo*. In the laser-induced CNV model, photocoagulation induced NF- κ B activation including nuclear translocation of NF- κ B p65 and I κ B- α degradation. To confirm NF- κ B involvement in the treatment with GV1001, we used western blot analysis to evaluate the protein levels of I κ B- α that had to be degraded for nuclear NF- κ B translocation. Nuclear translocation of NF- κ B p65 was detected in choroidal vascular endothelial and RPE cells. The nuclear translocation and/or retention of NF- κ B p65 was markedly increased in vehicle-treated group as compared with normal controls ($P = 0.012$). It substantially decreased in 0.1 nM GV1001-treated group ($P = 0.008$), 1 nM GV1001-treated group ($P = 0.008$), and 10 nM GV1001-treated group ($P = 0.008$, Figure 6). Levels of I κ B- α protein from the homogenized RPE-choroid complex were significantly reduced in vehicle-treated group as compared with normal controls that did not induce CNV ($P = 0.048$). These effects were partially reversed by treatment with GV1001 at the dose of 1 nM ($P = 0.048$). Levels

of phospho-I κ B- α protein from the homogenized RPE-choroid complex were significantly increased in vehicle-treated group compared with normal controls that did not induce CNV ($P = 0.014$). These effects were reversed by treatment with GV1001 at the dosage of 0.1 ($P = 0.048$) and 1 nM ($P = 0.032$). Levels of phospho-NF- κ B p65 protein from the homogenized RPE-choroid complex were also significantly increased in vehicle-treated group as compared with normal controls that did not induce CNV ($P = 0.020$). These effects were reversed by treatment with GV1001 at the dosage of 1 nM ($P = 0.035$, Figure 7). Therefore, GV1001 significantly inhibited the phosphorylation of I κ B- α and NF- κ B p65 subunit as well as nuclear translocation of NF- κ B p65.

Effect of GV1001 on pro-inflammatory cytokines production

To determine whether GV1001 treatment affects angiogenic and inflammatory molecules related to the pathogenesis of CNV, protein levels of IL-1 β , IL-6, VEGF, MCP-1, and TNF- α in the homogenized RPE-choroid complex were analyzed by Multiplex immunoassay. Since the CNV inhibitory effect was most effective at the concentration of 1 nM, we determined the effect of 1 nM of GV1001 to investigate the possible underlying molecular mechanisms. Protein levels of IL-1 β , IL-6, and VEGF in the RPE-choroid complex were significantly higher in rats with CNV than in normal controls (Figure 8). Treatment with 1 nM GV1001 significantly suppressed protein levels of IL-1 β (167.0 ± 6.3 pg/mg vs. 128.7 ± 4.5 pg/mg, $P < 0.001$), IL-6 (498.0 ± 5.4 pg/mg vs. 309.6 ± 12.8 pg/mg, $P < 0.001$), and VEGF (407.1 ± 17.8 pg/mg vs. 337.4 ± 14.1 pg/mg, $P = 0.005$) as compared to vehicle treatment. The three groups did not differ significantly in terms of MCP-1 and TNF- α levels in the

RPE-choroid complex.

Telomerase activity in CNV

To determine whether the inhibitory mechanism of GV1001 is related to the telomerase activity in CNV, immunohistochemical analysis was performed using paraffin-embedded serial sections containing the center of the CNV lesion. However, hTERT expression could not be confirmed in comparison with the negative control (Figure 9).

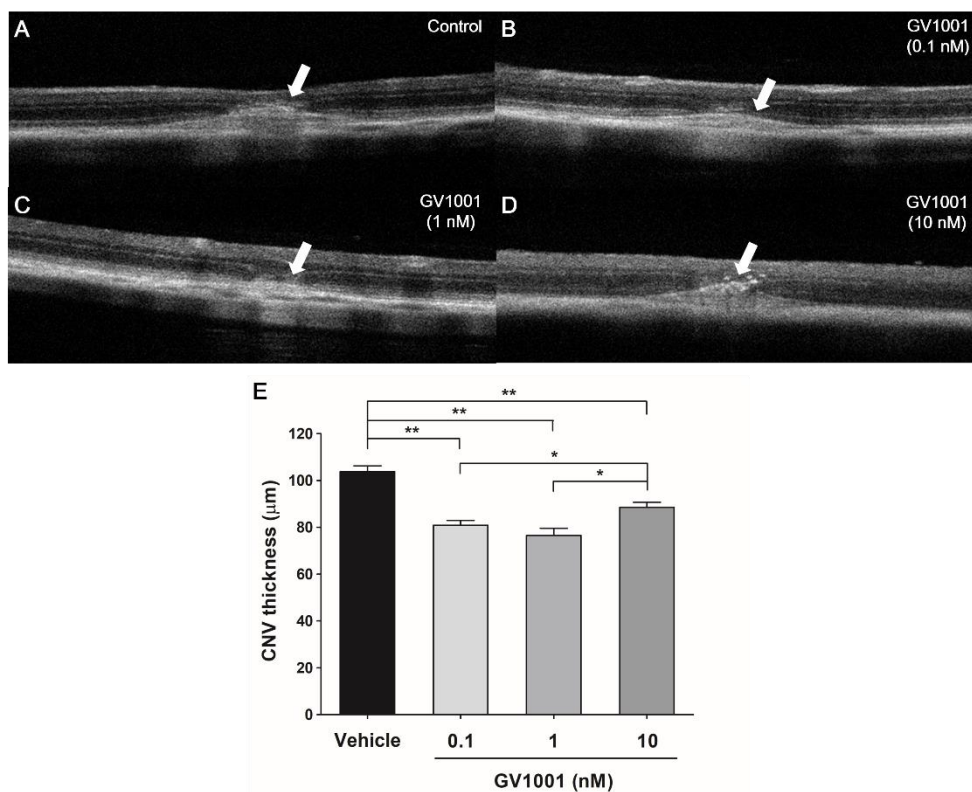


Figure 3. Spectral-domain optical coherence tomography images of CNV. (A) Vehicle-treated group. (B) 0.1 nM GV1001-treated group. (C) 1 nM GV1001-treated group. (D) 10 nM GV1001-treated group. White arrows indicate the spindle-shaped CNV lesion. (E) Measurement of CNV thickness, *in vivo*, showed significantly smaller CNV in GV1001-treated groups than in vehicle-treated group. Data are presented as mean \pm standard deviation. * $P < 0.05$, ** $P < 0.001$. (Mann-Whitney *U* test)

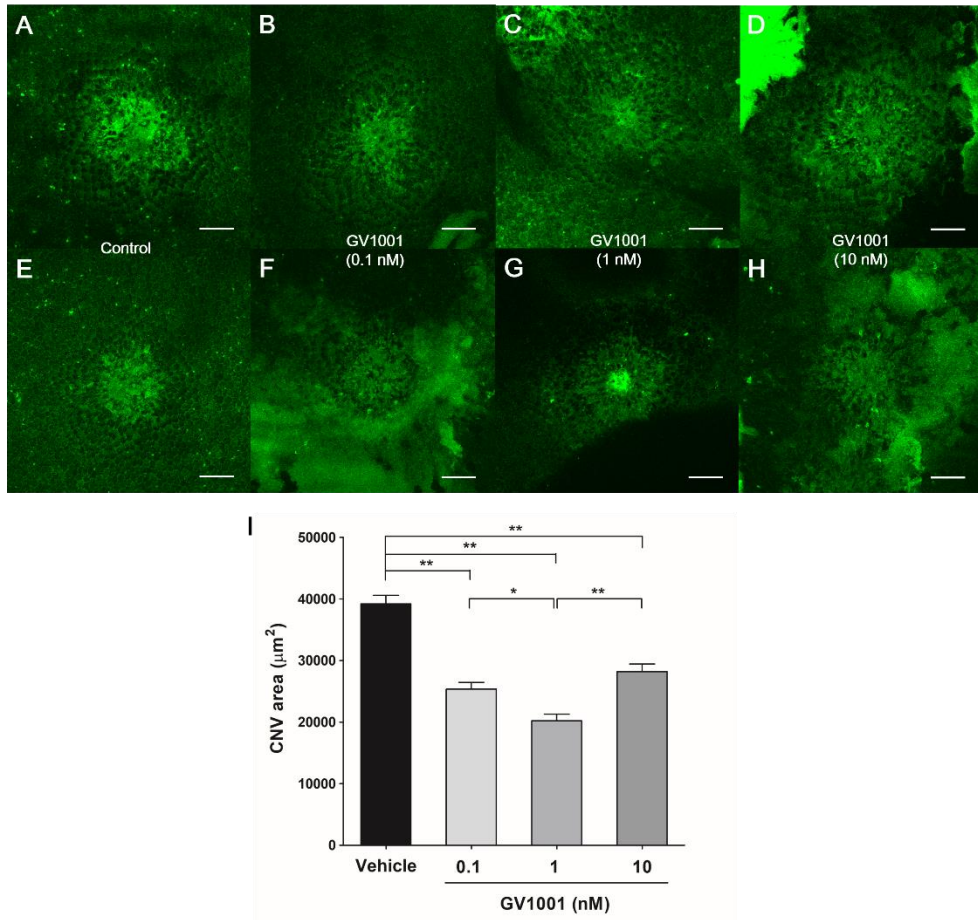


Figure 4. Fluorescent images of CNV in retinal pigment epithelium-choroid-scleral flat mounts. (A, E) Vehicle-treated group. (B, F) 0.1 nM GV1001-treated group. (C, G) 1 nM GV1001-treated group. (D, H) 10 nM GV1001-treated group. The scale bar represents 100 μm. (I) Mean CNV area was significantly lower in GV1001-treated groups than in vehicle-treated group. Data are presented as mean \pm standard deviation. * $P < 0.05$, ** $P < 0.001$. (Mann-Whitney U test)

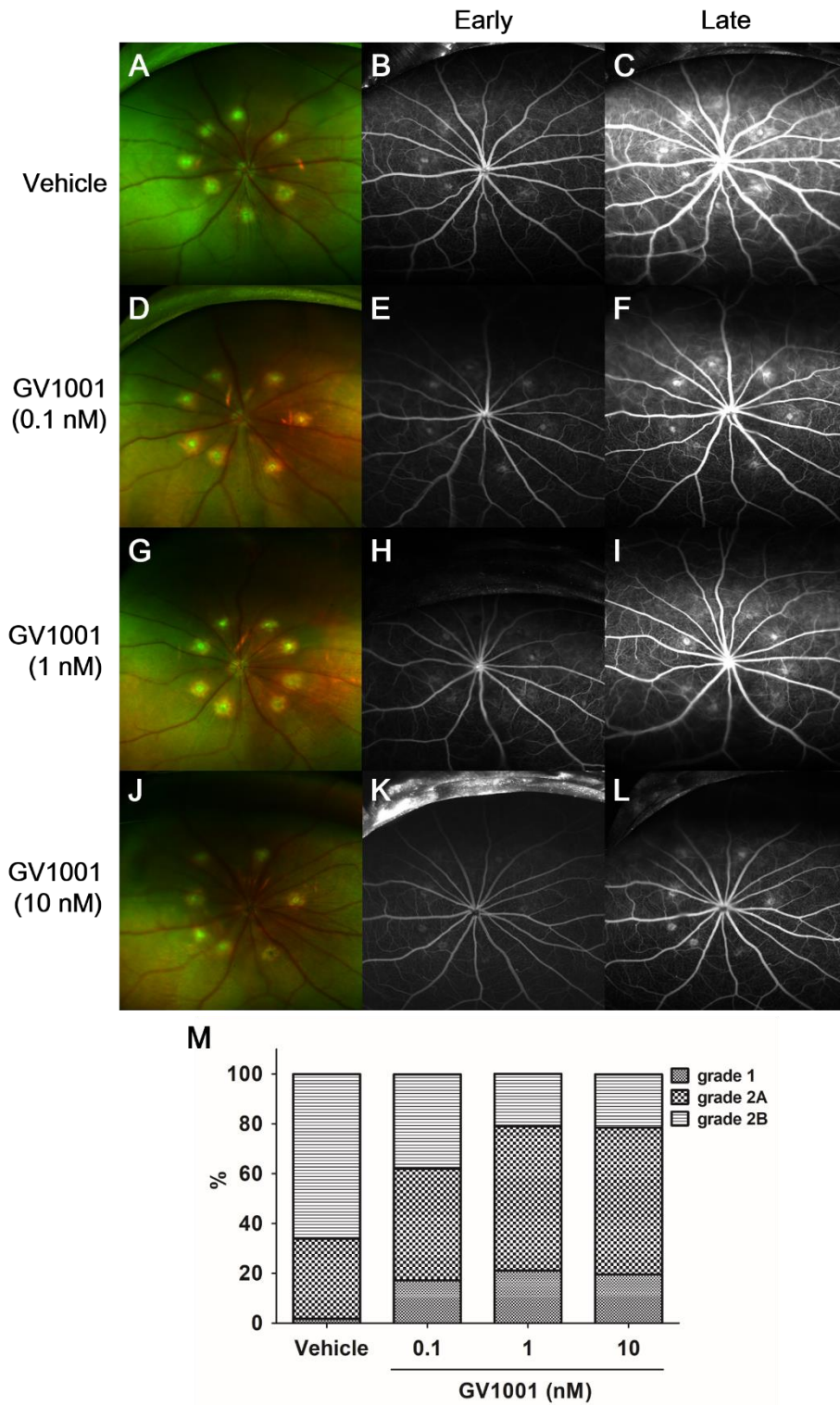


Figure 5. Fluorescein angiographic images. Fundus photographs (A, D, G, J), early

(B, E, H, K) and late phase (C, F, I, L) fluorescein angiographic images. (A, B, C) Vehicle-treated group. (D, E, F) 0.1 nM GV1001-treated group. (G, H, I) 1 nM GV1001-treated group. (J, K, L) 10 nM GV1001-treated group. (M) Histogram of angiographic leakage grades. Significantly fewer grade 2B lesions were observed in the GV1001-treated group than in vehicle-treated group.

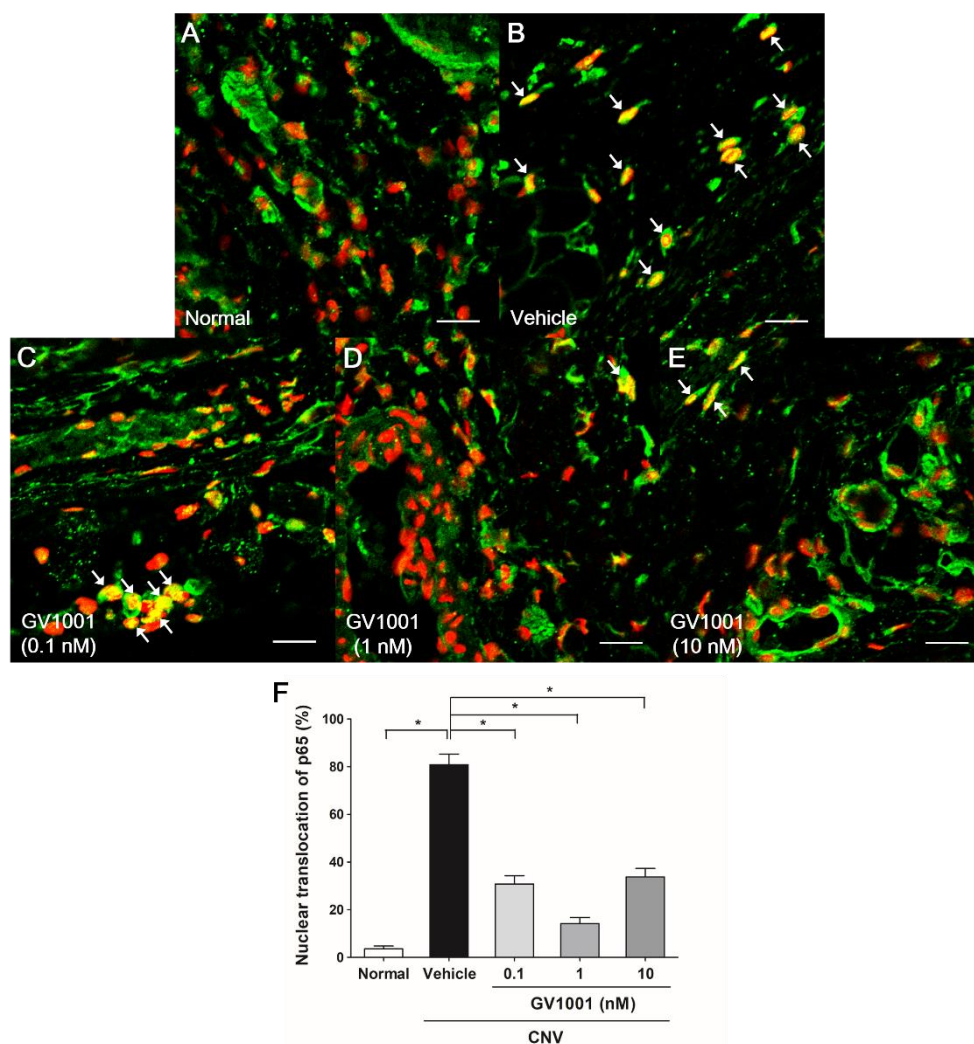


Figure 6. In vivo inhibition of nuclear translocation of NF-κB p65 by treatment with GV1001. (A) Normal controls. (B) Vehicle-treated group. (C) 0.1 nM GV1001-treated group. (D) 1 nM GV1001-treated group. (E) 10 nM GV1001-treated group. Nuclear localization of NF-κB p65 was visualized in the superimposed image showing *yellow* nuclei arising from the *green* fluorescence of the anti-NF-κB p65 antibody and *red* fluorescence from nuclei with TOTO-3. White arrows indicate p65 nuclear translocation in choroidal vascular endothelial cells and RPE cells. The scale bar represents 20 μm. (F) The nuclear translocation of NF-κB p65 was significantly

suppressed in GV1001-treated groups than in vehicle-treated group. Data are presented as mean \pm standard deviation. $*P < 0.05$. (Mann-Whitney U test)

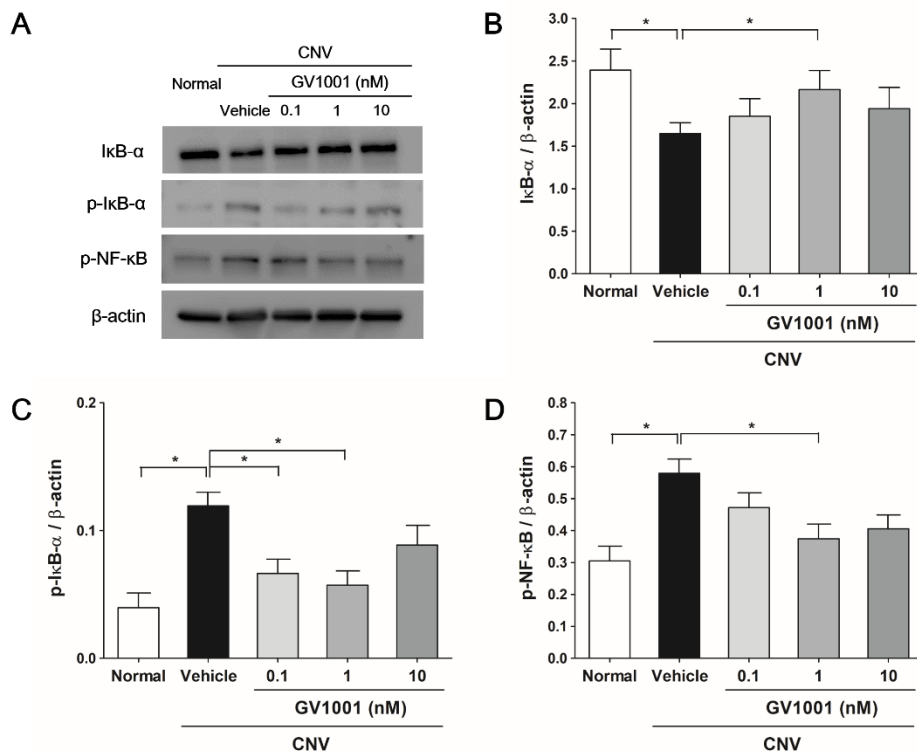


Figure 7. The suppression of NF-κB activation by treatment with GV1001. (A) Western blot showing IκB-α, phospho-IκB-α, and phospho-NF-κB p65 protein from the homogenized RPE-choroid complex. (B) 1 nM GV1001 suppressed IκB-α degradation in the RPE-choroid complex. (C) 0.1 and 1 nM GV1001 suppressed production of phospho-IκB-α. (D) 1 nM GV1001 suppressed production of phospho-NF-κB p65. Data are presented as mean ± standard deviation. * $P < 0.05$. (Mann-Whitney U test)

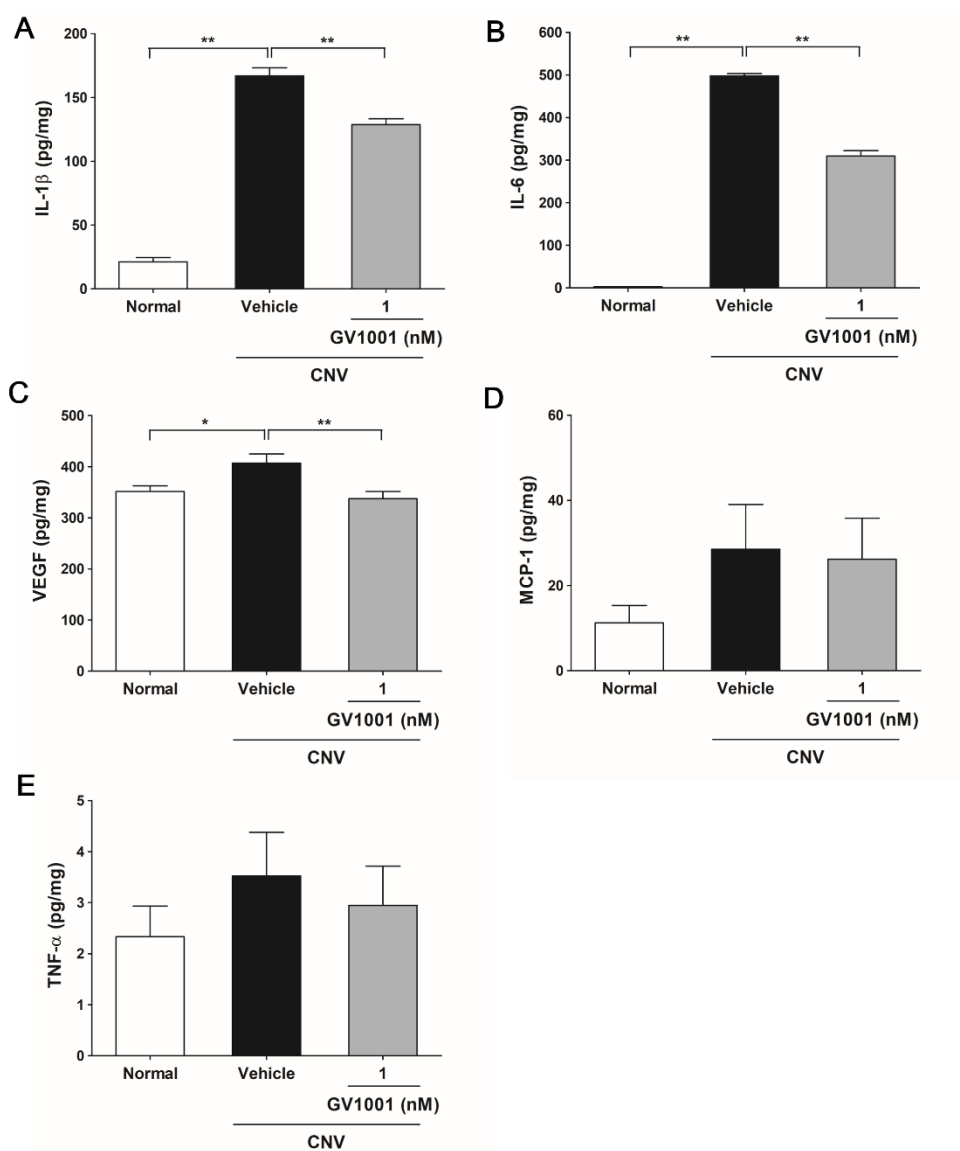


Figure 8. Quantification of IL-1 β , IL-6, VEGF, MCP-1, and TNF- α levels in RPE-choroid complex. GV1001 at 1 nM concentration significantly suppressed RPE-choroid protein levels of IL-1 β (A), IL-6 (B), and VEGF (C). The protein levels of MCP-1 (D) and TNF- α (E) were not significantly different among the three groups. Data are presented as mean \pm standard deviation. * P < 0.05, ** P < 0.001. (Mann-Whitney U test)

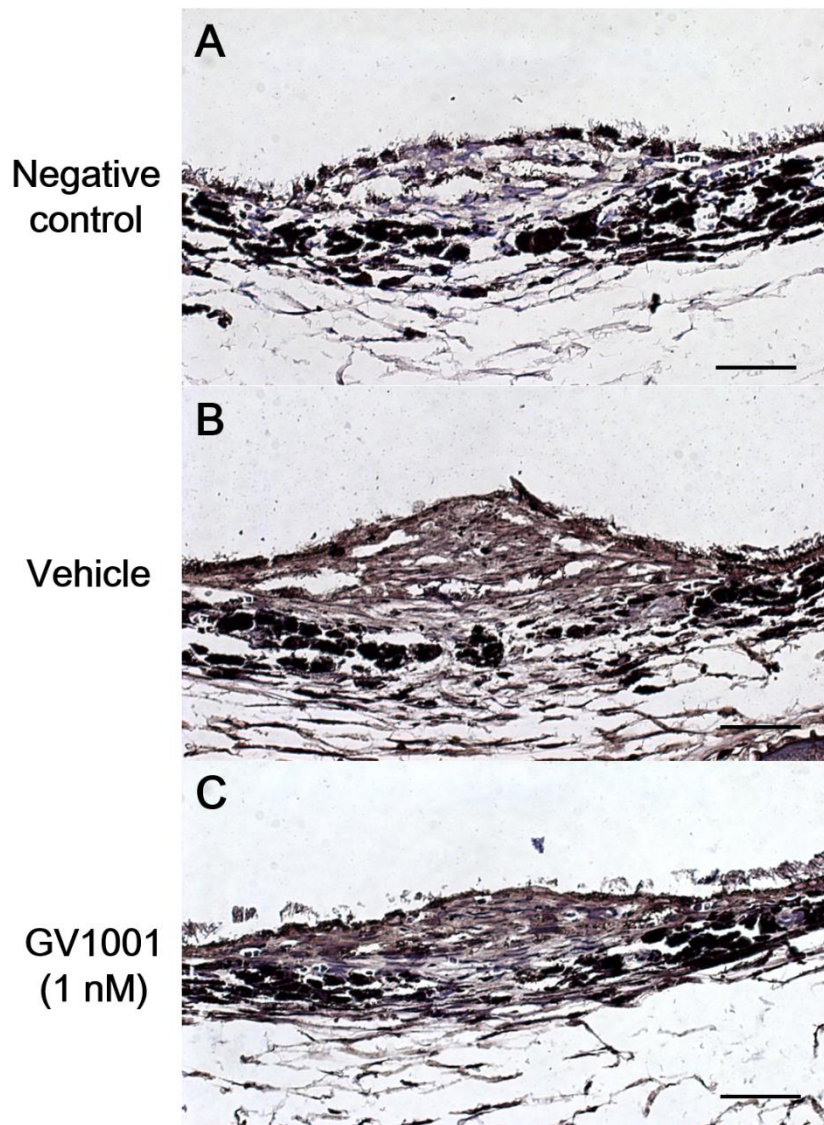


Figure 9. Immunohistochemical staining of hTERT expression in paraffin-embedded rat eye sections through areas of CNV. Brown staining indicates positive staining. (A) Negative control with no primary antibody. (B) Vehicle-treated group. (C) 1 nM GV1001-treated group. Scale bar indicates 50 μ m. hTERT was negative in all samples.

DISCUSSION

In the current study, we demonstrated a novel role of GV1001 in modulating the inflammatory pathways and inhibiting laser-induced CNV in rat model. Experimental CNV led to inflammatory cascade reaction, possibly through the activation of NF- κ B signaling, and these changes were notably reduced following GV1001 administration. These data suggested that GV1001 might exert its inhibitory effects on CNV through suppressing NF- κ B signaling.

GV1001 was first developed as an anticancer peptide vaccine.³⁷ It has been proven to be safe in several phase I or II clinical trials in patients with various cancers.^{13,15-17} Furthermore, Lee et al.²⁷ reported a surprising function of GV1001 as a cell-penetrating peptide. They demonstrated that it can penetrate various cell membranes, accumulate in the cytoplasm, and has the potential to have a direct *in vitro* effect, in addition to inducing an anticancer immune response. Moreover, GV1001 was subsequently revealed to function as an anti-inflammatory agent. In a mouse renal ischemia-reperfusion injury model, this peptide significantly reduced infiltration of neutrophils and macrophages in the kidney.³² Choi et al.³⁸ reported that GV1001 reduced the clinical joint scores, serum IL-6 levels, and histological joint scores in a mouse model of rheumatoid arthritis. These results suggest that GV1001 may be an effective therapeutic agent in the management of inflammation.

Although the detailed molecular and cellular mechanisms underlying CNV are not fully elucidated, inflammation and NF- κ B signaling proved to be critical factors to promote CNV formation. Previous studies have shown that inhibition of pro-inflammatory cytokines such as IL-1 β ,¹ IL-6,² VEGF,³⁶ MCP-1,³⁹ and TNF- α ⁴

resulted in suppression of CNV. Izumi-Nagai et al.^{40,41} investigated the role of NF- κ B activation on CNV development. They showed that carotenoids, such as lutein or astaxanthin, suppressed the activation of the NF- κ B pathway, including I κ B- α degradation and p65 nuclear translocation, resulting in significant suppression of CNV development. The current results demonstrated for the first time that, GV1001-treated group had smaller CNV size and less fluorescence leakage than the vehicle-treated group, which suggests that GV1001 can effectively suppress the experimental CNV. To investigate the possible molecular mechanism underlying GV1001 suppression in CNV, we evaluated the NF- κ B signaling pathway and inflammation-associated molecules. After I κ B phosphorylation and degradation—that is attributable to injury or inflammation in the laser injured retina—NF- κ B p65/p50 enters the nucleus and binds to the κ B sequence, thereby promoting the transcription of target genes including pro-inflammatory factors and cell adhesion molecules.^{42,43} In the present study, we demonstrated that GV1001 inhibited activation of NF- κ B by suppressing degradation of I κ B and nuclear translocation of NF- κ B p65 in the RPE-choroid of the CNV rat model (Figure 10). It is noteworthy that the protein levels of IL-1 β , IL-6, and VEGF were significantly decreased in GV1001-treated group, although the results were not significant for MCP-1 and TNF- α . Therefore, our results suggest that the CNV inhibitory effect of GV1001 is primarily via anti-inflammatory activity by regulation of NF- κ B signaling activation and modulation of its associated cytokines, such as IL-1 β , IL-6, and VEGF.

Meanwhile, it remains unknown what specific cell types are involved in the mechanism by which GV1001 inhibits CNV. Moreover, it has not yet been determined which receptor in retina interacts with GV1001 or whether GV1001 can

penetrate RPE and choroidal endothelial cells or not. However, it can be speculated from the previous literature. Paimela et al.⁴⁴ revealed that HSP70 is a significant regulator of the NF- κ B pathway and consequently of the IL-6 expression in human adult retinal pigment epithelial cells (ARPE-19). They revealed that following lipopolysaccharides-stimulus, APRE-19 cells exhibited significant increase in phosphorylated NF- κ B at serine 536 when compared to untreated cells, and this effect was attenuated by the pre-treatment with celastrol, a quinone methide triterpene drug in the treatment of various inflammatory and autoimmune diseases. Amirkavei et al.⁴⁵ investigated the heat shock response by measuring the expression levels of HSP70 in the mouse RPE. They suggested that heat shock response to transpupillary laser-induced heating showed a ring-shaped expression of HSP70 with very strong expression at the border of the heated area and a weak or negligible expression in the center of the laser spot. It is possible that GV1001 may interact with HSP70 in RPE cells induced in response to laser-induced CNV and internalize into cells by HSP-mediated endocytosis, but the detailed mechanism requires further investigation.

Dosage response of GV1001 treatment showed that the concentration of 1 nM had the highest inhibitory effect on CNV size. Since the optimum concentration of GV1001 for laser-induced CNV rat model has not yet been established, we performed several pilot studies. We found that less than 0.1 nM of GV1001 was not significantly effective to inhibit CNV; thus, we selected 0.1 nM, 1 nM, and 10 nM concentrations for this study. Chang et al.⁴⁶ revealed that high concentration-GV1001 group showed less protective effects against ischemia-reperfusion injury after lung transplantation in rats. They speculated the reason for less effective anti-

inflammatory results in high concentration group is its high concentration and viscous characteristics. The underlying cause for lack of dose-response in this study is not known. However, the following hypotheses are offered. Firstly, the concentration distribution of GV1001 tested in this study may be insufficient to determine dose-related response. It might be necessary to repeat experiments, by including more variations with respect to GV1001 concentrations, and at smaller increments as those used for this experiment. Secondly, because the development and growth of CNV is a complex and dynamic process that involves angiogenesis, oxidative stress, inflammation, and immune mechanisms, a small number of samples may be affected by factors other than GV1001 itself. Large-scale experiments after controlling for confounding factors will be needed. Thirdly, due to the nature of the peptide drug, the dose response may not be evident in high concentration.⁴⁷ Proteolytic degradation of peptide drugs leave the core peptide, which exerts the drug effect. Degradation may be delayed in high concentration, and thus the dose response of the peptide drug may not be apparent.

GV1001 may rapidly degrade before uptake by APCs, and peptide presentation in a non-inflammatory environment may induce tolerance rather than immunity. The relevance between concentration used and the various function of GV1001 has not been clearly identified, but it is presumed to trigger immunity and exert anti-cancer effect when used at high concentrations and exert anti-inflammatory effect when used at low concentrations. In a Phase I/II clinical trials with GV1001, the concentrations of GV1001 injected with adjuvant granulocyte macrophage-colony stimulating factor (GM-CSF) were mainly 112 µg, 560 µg, and 1.87 mg per injection.^{13,15-18,37} The concentrations of GV1001 used in animal models

to investigate the anti-inflammatory effect were 5 and 50 pmol/kg in rheumatoid arthritis model,³⁸ and 1000 nM in renal ischemic reperfusion injury model.³² Although human clinical trial of GV1001 in inflammatory disease has not yet been performed, further studies on the various functions of GV1001 depending on the concentration should be supported.

In the present study, the CNV inhibiting effect of intravitreal injections of aflibercept was compared with that of subcutaneous injections of GV1001 to investigate the clinical significance. Intravitreal injections of aflibercept (80 µg/2 µL; Bayer Pharma AG, Berlin, Germany) was administered 7 days after laser photocoagulation. Although choroidal flat mounts showed significantly smaller mean CNV area in the aflibercept-treated group ($16,030.20 \pm 6,506.87 \mu\text{m}^2$) than that in the 1 nM GV1001-treated group ($20,214.42 \pm 7,417.81 \mu\text{m}^2$, $P = 0.032$), histological analysis revealed that the largest CNV lesion diameter was not significantly different between the aflibercept-treated group ($42.35 \pm 5.49 \mu\text{m}$) and 1 nM GV1001-treated group ($43.07 \pm 10.40 \mu\text{m}$, $P = 0.785$) (Figure 11). Therefore, even though further comparison experiments with more precise settings are required, GV1001 seems to have an effect comparable to that of aflibercept with respect to inhibition of laser-induced CNV.

There are some limitations to the present study. First, in addition to vehicle control, there was no negative control using scrambled peptides that have sequences similar to but different from those of GV1001. When the CNV inhibitory effect was not evident in the scrambled peptide control group, the results of this study would have been able to discriminate that the CNV inhibitory effect was the true effect of GV1001 and not the effect of the peptide drug. Second, with regard to CNV

suppression, experiments at the level of the RPE or choroidal endothelial cells were not conducted. Although the present study revealed that the NF- κ B pathway and the modulation of inflammatory cytokines are involved in the mechanism by which GV1001 inhibits CNV, it was not determined which cells in the retina and choroid layer GV1001 interacts with and exerts its effect. Third, FITC-conjugated GV1001 was not used in current study. If FITC-conjugated GV1001 was used instead of hTERT in immunohistochemical staining, the localization of GV1001 could be better investigated and the cellular mechanism involved in the mode of action could be identified.

Although the current treatment of neovascular AMD with intravitreal anti-VEGF injection offers tremendous value to many patients, there are still risks of severe adverse effects associated with multiple injections, including endophthalmitis⁴⁸ or retinal detachment.⁴⁹ Contrastingly, targeting NF- κ B signaling pathway via blunt excessive upregulation of pro-inflammatory factors, can be a promising strategy in treatment of neovascular AMD. Firstly, GV1001 can be administered systemically via the intradermal injection, and has a good safety and tolerability profile in human clinical trials. Secondly, highly purified peptides have advantages over full-length proteins in that peptides are easily synthesized without the risk of infection by recombinant viruses or exposure to exogenous allergens. Additionally, GV1001 and anti-VEGF treatments could have synergistic properties and, together, have the potential to reduce the economic burdens and clinical risks related to repeated intravitreal injections. The concomitant therapy with intravitreal anti-VEGF and systemic GV1001 would merit further human studies. In addition, it will be an interesting topic to investigate that GV1001 still exhibit a valid CNV

inhibitory effect through intravitreal injection in animal model. This is valuable in that it is a route of administration which is consistent with the established anti-VEGF treatment. Although the risk of intravitreal injection described above still exists, if it acts more directly in the local environment than in the systemic administration through intradermal injection and shows more potent efficacy in CNV inhibition, the relevance in human clinical trials as a novel therapeutic strategy for neovascular AMD will increase further.

In conclusion, the results presented here, suggest that GV1001 significantly inhibits CNV development in rats. This could be associated with its anti-inflammatory activity by regulation of NF- κ B signaling activation and modulation of IL-1 β , IL-6, and VEGF. Our current data may provide molecular evidence of potential validity of GV1001 treatment as a reasonable therapeutic adjuvant strategy for treating neovascular AMD.

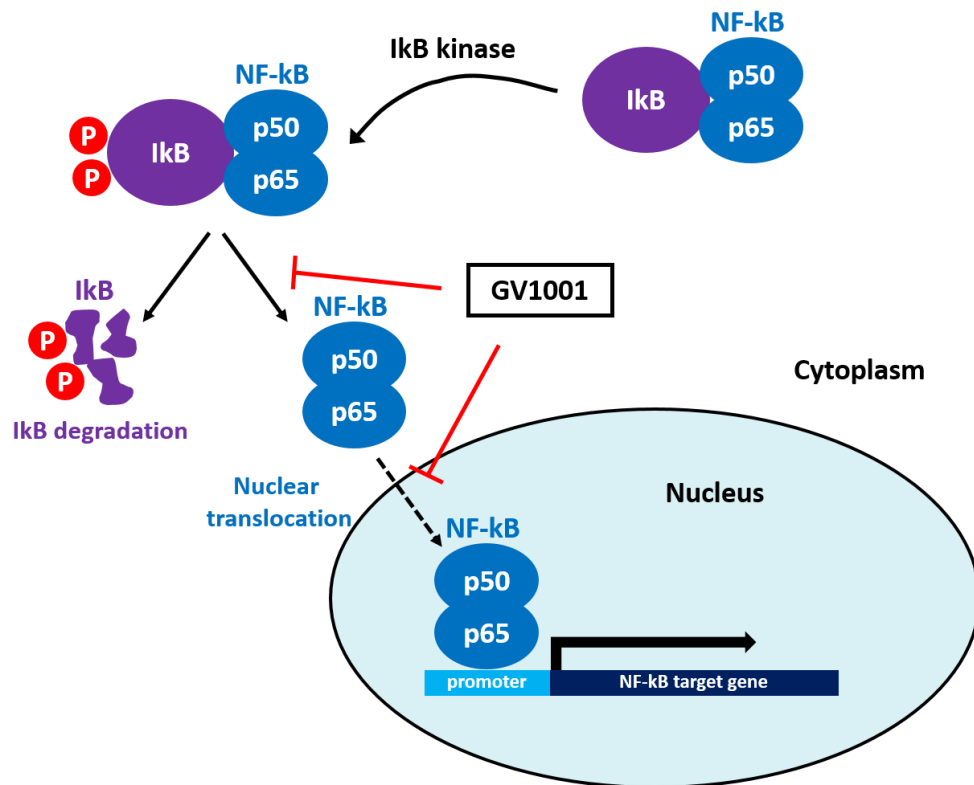


Figure 10. Schematic diagram of the NF- κ B signaling pathway suppressed by GV1001. GV1001 inhibited the NF- κ B activation via the prevention of I κ B phosphorylation and degradation and NF- κ B p65 nuclear translocation.

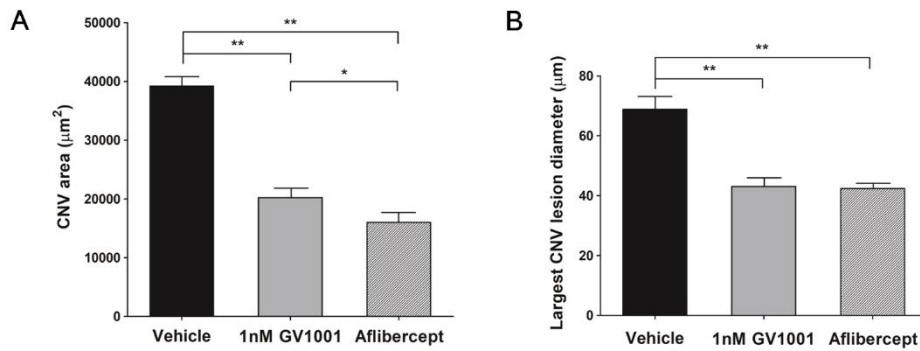


Figure 11. Comparison of the mean CNV area and the mean largest CNV lesion diameter between GV1001-treated group and aflibercept-treated group. (A) Choroidal flat mounts showed significantly smaller mean CNV area in the aflibercept-treated group than that in the 1 nM GV1001-treated group. (B) Histological analysis revealed that the largest CNV lesion diameter was not significantly different between the aflibercept-treated group and 1 nM GV1001-treated group. Data are presented as mean \pm standard deviation. * $P < 0.05$, ** $P < 0.001$. (Mann-Whitney U test)

REFERENCES

1. Lavalette S, Raoul W, Houssier M, et al. Interleukin-1beta inhibition prevents choroidal neovascularization and does not exacerbate photoreceptor degeneration. *Am J Pathol.* 2011;178:2416-23.
2. Izumi-Nagai K, Nagai N, Ozawa Y, et al. Interleukin-6 receptor-mediated activation of signal transducer and activator of transcription-3 (STAT3) promotes choroidal neovascularization. *Am J Pathol.* 2007;170:2149-58.
3. Yamada K, Sakurai E, Itaya M, et al. Inhibition of laser-induced choroidal neovascularization by atorvastatin by downregulation of monocyte chemotactic protein-1 synthesis in mice. *Invest Ophthalmol Vis Sci.* 2007;48:1839-43.
4. Shi X, Semkova I, Muther PS, et al. Inhibition of TNF-alpha reduces laser-induced choroidal neovascularization. *Exp Eye Res.* 2006;83:1325-34.
5. Shaw VE, Naisbitt DJ, Costello E, et al. Current status of GV1001 and other telomerase vaccination strategies in the treatment of cancer. *Expert Rev Vaccines.* 2010;9:1007-16.
6. Nakamura TM, Morin GB, Chapman KB, et al. Telomerase catalytic subunit homologs from fission yeast and human. *Science.* 1997;277:955-9.
7. Kim NW, Piatyszek MA, Prowse KR, et al. Specific association of human telomerase activity with immortal cells and cancer. *Science.* 1994;266:2011-5.
8. Tahara H, Yasui W, Tahara E, et al. Immuno-histochemical detection of human telomerase catalytic component, hTERT, in human colorectal tumor and non-tumor tissue sections. *Oncogene.* 1999;18:1561-7.
9. Sahin E, Depinho RA. Linking functional decline of telomeres,

mitochondria and stem cells during ageing. *Nature*. 2010;464:520-8.

10. Greenberg RA, Chin L, Femino A, et al. Short dysfunctional telomeres impair tumorigenesis in the INK4a(Δ 2/3) cancer-prone mouse. *Cell*. 1999;97:515-25.
11. Harley CB. Telomerase and cancer therapeutics. *Nat Rev Cancer*. 2008;8:167-79.
12. Stevenson CL. Advances in peptide pharmaceuticals. *Curr Pharm Biotechnol*. 2009;10:122-37.
13. Bernhardt SL, Gjertsen MK, Trachsel S, et al. Telomerase peptide vaccination of patients with non-resectable pancreatic cancer: A dose escalating phase I/II study. *Br J Cancer*. 2006;95:1474-82.
14. Middleton G, Ghaneh P, Costello E, et al. New treatment options for advanced pancreatic cancer. *Expert Rev Gastroenterol Hepatol*. 2008;2:673-96.
15. Kyte JA, Gaudernack G, Dueland S, et al. Telomerase peptide vaccination combined with temozolomide: a clinical trial in stage IV melanoma patients. *Clin Cancer Res*. 2011;17:4568-80.
16. Brunsvig PF, Kyte JA, Kersten C, et al. Telomerase peptide vaccination in NSCLC: a phase II trial in stage III patients vaccinated after chemoradiotherapy and an 8-year update on a phase I/II trial. *Clin Cancer Res*. 2011;17:6847-57.
17. Brunsvig PF, Aamdal S, Gjertsen MK, et al. Telomerase peptide vaccination: a phase I/II study in patients with non-small cell lung cancer. *Cancer Immunol Immunother*. 2006;55:1553-64.
18. Greten TF, Forner A, Korangy F, et al. A phase II open label trial evaluating safety and efficacy of a telomerase peptide vaccination in patients with advanced

hepatocellular carcinoma. BMC Cancer. 2010;10:209.

19. Kyte JA. Cancer vaccination with telomerase peptide GV1001. Expert Opin Investig Drugs. 2009;18:687-94.

20. Kim BK, Kim BR, Lee HJ, et al. Tumor-suppressive effect of a telomerase-derived peptide by inhibiting hypoxia-induced HIF-1 α -VEGF signaling axis. Biomaterials. 2014;35:2924-33.

21. Ellis RJ. Protein misassembly: macromolecular crowding and molecular chaperones. Adv Exp Med Biol. 2007;594:1-13.

22. Robert J, Menoret A, Cohen N. Cell surface expression of the endoplasmic reticular heat shock protein gp96 is phylogenetically conserved. J Immunol. 1999;163:4133-9.

23. Eustace BK, Jay DG. Extracellular roles for the molecular chaperone, hsp90. Cell Cycle. 2004;3:1098-100.

24. Tsutsumi S, Neckers L. Extracellular heat shock protein 90: a role for a molecular chaperone in cell motility and cancer metastasis. Cancer Sci. 2007;98:1536-9.

25. Lindquist S, Craig EA. The heat-shock proteins. Annu Rev Genet. 1988;22:631-77.

26. Suto R, Srivastava PK. A mechanism for the specific immunogenicity of heat shock protein-chaperoned peptides. Science. 1995;269:1585-8.

27. Lee SA, Kim BR, Kim BK, et al. Heat shock protein-mediated cell penetration and cytosolic delivery of macromolecules by a telomerase-derived peptide vaccine. Biomaterials. 2013;34:7495-505.

28. Kim JW, Yadav DK, Kim SJ, et al. Anti-cancer effect of GV1001 for

- prostate cancer: function as a ligand of GnRHR. *Endocr Relat Cancer*. 2019;26:147-62.
29. Park HH, Lee KY, Kim S, et al. Novel vaccine peptide GV1001 effectively blocks beta-amyloid toxicity by mimicking the extra-telomeric functions of human telomerase reverse transcriptase. *Neurobiol Aging*. 2014;35:1255-74.
30. Lee YK, Nata'atmaja BS, Kim BH, et al. Protective effect of telomerase-based 16-mer peptide vaccine (GV1001) on inferior epigastric island skin flap survivability in ischaemia-reperfusion injury rat model. *J Plast Surg Hand Surg*. 2017;51:210-16.
31. Chang JE, Kim HJ, Jheon S, Lim C. Protective effects of GV1001 on myocardial ischemiareperfusion injury. *Mol Med Rep*. 2017;16:7315-20.
32. Koo TY, Yan JJ, Yang J. Protective effect of peptide GV1001 against renal ischemia-reperfusion injury in mice. *Transplant Proc*. 2014;46:1117-22.
33. Choi J, Kim H, Kim Y, et al. The Anti-inflammatory Effect of GV1001 Mediated by the Downregulation of ENO1-induced Pro-inflammatory Cytokine Production. *Immune Netw*. 2015;15:291-303.
34. Ko YJ, Kwon KY, Kum KY, et al. The Anti-Inflammatory Effect of Human Telomerase-Derived Peptide on *P. gingivalis* Lipopolysaccharide-Induced Inflammatory Cytokine Production and Its Mechanism in Human Dental Pulp Cells. *Mediators Inflamm*. 2015;2015:385127.
35. Rowe-Rendleman C, Glickman RD. Possible therapy for age-related macular degeneration using human telomerase. *Brain Res Bull*. 2004;62:549-53.
36. Krzystolik MG, Afshari MA, Adamis AP, et al. Prevention of experimental choroidal neovascularization with intravitreal anti-vascular endothelial growth

factor antibody fragment. *Arch Ophthalmol*. 2002;120:338-46.

37. Staff C, Mozaffari F, Frodin JE, et al. Telomerase (GV1001) vaccination together with gemcitabine in advanced pancreatic cancer patients. *Int J Oncol*. 2014;45:1293-303.

38. Choi IA, Choi JY, Jung S, et al. GV1001 immunotherapy ameliorates joint inflammation in a murine model of rheumatoid arthritis by modifying collagen-specific T-cell responses and downregulating antigen-presenting cells. *Int Immunopharmacol*. 2017;46:186-93.

39. Tsutsumi C, Sonoda KH, Egashira K, et al. The critical role of ocular-infiltrating macrophages in the development of choroidal neovascularization. *J Leukoc Biol*. 2003;74:25-32.

40. Izumi-Nagai K, Nagai N, Ohgami K, et al. Macular pigment lutein is antiinflammatory in preventing choroidal neovascularization. *Arterioscler Thromb Vasc Biol*. 2007;27:2555-62.

41. Izumi-Nagai K, Nagai N, Ohgami K, et al. Inhibition of choroidal neovascularization with an anti-inflammatory carotenoid astaxanthin. *Invest Ophthalmol Vis Sci*. 2008;49:1679-85.

42. Baldwin AS, Jr. The NF-kappa B and I kappa B proteins: new discoveries and insights. *Annu Rev Immunol*. 1996;14:649-83.

43. Baeuerle PA, Henkel T. Function and activation of NF-kappa B in the immune system. *Annu Rev Immunol*. 1994;12:141-79.

44. Paimela T, Hyttinen JM, Viiri J, et al. Celastrol regulates innate immunity response via NF-kappaB and Hsp70 in human retinal pigment epithelial cells. *Pharmacol Res*. 2011;64:501-8.

45. Amirkavei M, Pitkanen M, Kaikkonen O, et al. Induction of Heat Shock Protein 70 in Mouse RPE as an In Vivo Model of Transpupillary Thermal Stimulation. *Int J Mol Sci.* 2020;21.
46. Chang JE, Kim HJ, Yi E, et al. Reduction of ischaemia-reperfusion injury in a rat lung transplantation model by low-concentration GV1001. *Eur J Cardiothorac Surg.* 2016;50:972-79.
47. Lee AC, Harris JL, Khanna KK, Hong JH. A Comprehensive Review on Current Advances in Peptide Drug Development and Design. *Int J Mol Sci.* 2019;20.
48. Cheung CS, Wong AW, Lui A, et al. Incidence of endophthalmitis and use of antibiotic prophylaxis after intravitreal injections. *Ophthalmology.* 2012;119:1609-14.
49. Sampat KM, Garg SJ. Complications of intravitreal injections. *Curr Opin Ophthalmol.* 2010;21:178-83.

국문 초록

목적: 맥락막 신생혈관은 습성 연령관련황반변성의 특징적인 소견이다. 맥락막 신생혈관의 발생 기전에는 혈관내피성장인자(VEGF)와 관련된 혈관신생 자극뿐만 아니라 산화 스트레스와 염증 등이 복잡하게 관여한다. 본 연구에서는 인간 텔로머레이즈 유래 펩타이드인 GV1001이 실험적 맥락막 신생혈관에 미치는 영향에 대해 알아보려고 하였다.

방법: 실험적 맥락막 신생혈관은 Brown Norway 쥐에서 레이저로 유발하였다. GV1001은 각각 0.1 nM, 1 nM, 10 nM을 하루에 한번 피하로 주사하였으며, 레이저 유도 3일 전부터 레이저 유도 후 14일째까지 투약하였다. 맥락막 신생혈관을 분석하기 위하여 빛간섭단층촬영, 형광안저혈관조영술, 망막색소상피-맥락막 플랫 마운트를 시행하였다. GV1001의 작용 기전을 파악하기 위해, I κ B- α 단백질의 농도와 nuclear factor κ B (NF- κ B) 의 핵내 이동을 p65 면역조직화학 염색을 통해 평가하였다. 또한 interleukin (IL)-1 β , IL-6, VEGF, monocyte chemotactic protein (MCP)-1, tumor necrosis factor (TNF)- α 발현 정도를 측정하기 위하여 다중 면역 분석을 시행하였다.

결과: GV1001 투여군은 대조군에 비해 유의하게 맥락막 신생혈관의 두께가 낮고 ($P < 0.001$), 면적이 작았으며 ($P < 0.001$), 형광안저혈관조영술에서 임상적으로 유의한 혈관누출을 보이는 비율이 적었고 ($P < 0.001$), 1 nM 군에서 가장 큰 억제 효과를 보였다. 또한 GV1001 은 I κ B- α 분해 ($P < 0.05$)

와 NF- κ B p65 의 핵내 이동 ($P < 0.01$)을 억제하였고, 1 nM GV1001 처리시
에 IL-1 β ($P < 0.001$), IL-6 ($P < 0.001$), VEGF ($P = 0.005$) 발현을 유의하게 억
제하였다.

결론: GV1001 의 전신 투여가 레이저 유발 실험적 맥락막 신생혈관을 유
의하게 억제하는 것을 확인하였으며, 이는 NF- κ B 경로의 활성이 관여하
는 염증 기전 및 그로 인한 염증성 사이토카인의 발현 증가를 억제한 결
과로 추측된다. 본 연구를 통해 습성 연령관련황반변성의 보조적 치료
전략을 위한 새로운 약물 후보 물질의 잠재적 가능성을 확인하였다.

주요어: 연령관련황반변성, 맥락막 신생혈관, GV1001, NF- κ B 경로,
펩타이드, 텔로머레이즈, 백신

학번: 2013-31144

* 본 졸업 논문의 일부는 현재 Translational research (Lee EK, Kim YJ, Shon WJ, Yu HG. A telomerase-derived peptide vaccine inhibits laser-induced choroidal neovascularization in a rat model. Transl Res. 2020 Feb;216:30-42.) 에 출판 완료된 내용을 포함하고 있습니다.

* This work was supported in part by a grant of the Korea Health Technology R&D Project through the Korea Health Industry Development Institute (KHIDI), funded by the Ministry of Health & Welfare, Republic of Korea (grant number: HI14C1277). GemVax & KAEL provided the GV1001 peptide and a research grant (grant number: 800-20130362). GemVax & KAEL did not play any role in the study design, conduct of the study, or the collection, management, analysis, and interpretation of the data.